Planetary and Space Science 187 (2020) 104902

Contents lists available at ScienceDirect

Planetary and Space Science

journal homepage: www.elsevier.com/locate/pss

Ganymede's gravity, tides and rotational state from JUICE's 3GM experiment simulation

P. Cappuccio [a,*], A. Hickey [a], D. Durante [a], M. Di Benedetto [a], L. Iess [a], F. De Marchi [a], C. Plainaki [b], A. Milillo [c], A. Mura [c]

[a] Department of Mechanical and Aerospace Engineering, Sapienza University of Rome, Via Eudossiana, 18, 00184, Rome, Italy
[b] Italian Space Agency, Via del Politecnico snc, 00133, Rome, Italy
[c] Institute for Space Astrophysics and Planetology, Via del Fosso del Cavaliere, 100, 00133, Rome, Italy

A B S T R A C T

The JUpiter Icy Moons Explorer (JUICE) is a European Space Agency (ESA) mission that will launch in 2022 and arrive in the Jovian system in 2029 to investigate Jupiter's icy satellites. The mission will perform flybys of the icy moons Europa, Callisto and Ganymede before being inserted into a 280-day orbit around Ganymede: 150 days in Elliptical Orbit (GEO) followed by 130 days Circular Orbit at 500 km (GCO-500). During the orbital phase, JUICE will investigate the moon's surface, interior and exosphere, carrying out for the first time a complete characterization of an icy satellite. A suite of field and particle instruments will characterize the plasma and magnetic environment around the body. The 3GM experiment on board the spacecraft will exploit the GCO-500 phase to collect accurate Doppler and range measurements to determine the moon's orbit, gravity field and tide, therefore providing crucial information to accurately model its internal structure. The simulations carried out reveal that the moon's gravity field can be determined up to degree and order 40, depending on the magnitude of the gravity spectrum. The Love number k_2, modelling the gravitational response to eccentricity-driven, time-variable gravity gradient from Jupiter, is determined with an accuracy of $\sigma_{k_2} \sim 10^{-4}$. The obliquity, φ, and the libration at orbital period, ϕ, can be retrieved with a level of uncertainty of 1 and 2 μrad, respectively. Because of the 97 m^2 solar panels and the ensuing large area-to-mass ratio, JUICE will be affected by neutral particle drag. Here, we also assess the potential effect of spacecraft drag due to Ganymede's tenuous exosphere, which ranges between $10^{-17} - 10^{-16}$ kg/m^3 and generates an average drag of $\sim 4 \cdot 10^{-12}$ m/s^2, in the GCO-500 phase.

1. Introduction

Ganymede is the largest moon in our Solar System and with a radius of 2634 km it is even bigger than Mercury, although having a mass of less than one half of the Hermean planet. Among all the solid bodies in the Solar System Ganymede has the smallest normalized polar moment of inertia, $C/MR^2 = 0.3105 \pm 0.0028$ (Showman and Malhotra, 1999), implying that the body's mass is more concentrated towards the core (Anderson et al., 1999). According to this model, the moon's interior is fully differentiated with a metallic iron core, a spherical mantle and a thick water-ice shell. Ganymede is also the only moon known to have its own magnetic field (Kivelson et al., 1996). The gravity data available from the Galileo mission (Anderson et al., 1999) provided only weak constraints on its internal structure and the dynamo that is generating the magnetic field (Kimura et al., 2009). Ganymede's orbital period, eccentricity and semimajor axis are respectively 172 h (about 7 days), 0.0013 and 15 Jupiter radii. Being tidally locked to Jupiter, it is in synchronous rotation, like all other Galilean moons. As primarily observed by Galileo and subsequently described by Laplace, Ganymede's orbital period is in a 1:2:4 resonance with those of Io and Europa (the so-called Laplace resonance). The current knowledge of the moon's internal structure and the measured magnetic field are compatible with the presence of a subsurface ocean (McCord et al., 2001; Saur et al., 2015). However, an unambiguous detection of a global ocean beneath the icy surface requires better estimates of the moon's gravity field and gravitational tides, controlled by the Love number k_2. The determination of k_2 and the tidal quality factor, Q, will be crucial to understand the total energy budget of the moon (Showman et al., 1997; Showman and Malhotra, 1997).

JUICE (JUpiter Icy Moons Explorer) is an ESA L-class mission that will carry out a thorough investigation of the Jovian system, with a primary focus on Ganymede, the main scientific objective of the mission. The high level mission goals cover two main themes of the agency's Cosmic Vision 2015–2025: 'What are the conditions for the planet formation and emergence of life?' and 'How does the Solar System work?' (Grasset et al., 2013). Following its launch in June 2022, the spacecraft will spend 7.5 years in the cruise phase, which comprises a series of gravity assists (Earth-Venus-Earth-Mars-Earth) to shape its trajectory toward Jupiter. After the Jupiter Orbit Insertion (JOI) in January 2030, JUICE will spend

* Corresponding author.
E-mail address: paolo.cappuccio@uniroma1.it (P. Cappuccio).

https://doi.org/10.1016/j.pss.2020.104902
Received 18 November 2019; Received in revised form 4 February 2020; Accepted 12 March 2020
Available online 17 March 2020

3.3 years gathering data in the Jovian system, investigating the planet's magnetosphere and atmosphere, and performing multi-disciplinary observations of Europa, Callisto and Ganymede through its suite of scientific instrumentation. The JUICE nominal tour entails 2 flybys of Europa, 12 of Callisto, 15 of Ganymede and will end up with an extensive orbital phase around Ganymede. The latter actually consists of two sub-phases: the Ganymede Elliptical Orbit (GEO) and the Ganymede Circular Orbit (GCO). This will be the first time a moon other than Earth's Moon will be orbited by a spacecraft.

In this paper we present the results of numerical simulations showing the accuracies that can be achieved from the 3GM (Geodesy and Geophysics of Jupiter and the Galilean Moons) radio science experiment onboard the JUICE mission in the estimation of Ganymede's gravity field, tidal response and rotation. Our analysis includes the effect of non-gravitational accelerations due to the on-board propellant sloshing and the moon's tenuous exosphere, observed in the 1990's by the Galileo spacecraft (Barth et al., 1997; Ip et al., 1997) and by the Hubble Space Telescope (Hall et al., 1998). In Section 2 we describe the Ganymede gravity experiment and the 3GM payload; Section 3 outlines the dynamical model of the JUICE spacecraft while Section 4 describes the simulation setup. Finally, in Sections 5 and 6 we discuss the results and provide the conclusions of our analysis.

2. 3GM experiment on board the JUICE mission

3GM is one of the eleven experiments that JUICE will perform to study Jupiter and its moons Europa, Callisto and Ganymede. Passing close to Europa twice, JUICE aims to determine whether its interior is in hydrostatic equilibrium. If this hypothesis is verified the ratio of its low-degree gravity coefficients, at first order, shall be $J_2/C_{22} = 10/3$ (Matsuyama and Nimmo, 2009). The Callisto flybys will be used to infer the gravity field to at least degree and order 3 (Titov et al., 2014), though JUICE is expected to exceed this mission requirement and determine the moon's gravity with higher spatial resolution (Cappuccio et al., 2018; Di Ruscio et al., 2019). Along with the gravity field, 3GM could also infer Callisto's tidal response, controlled by the Love number k_2, which is crucial to unambiguously detect the presence of a liquid ocean under the outer ice shell of the moon (Moore and Schubert, 2003). 3GM observations of Ganymede will be carried out during the 4-month GCO-500 phase (a 101-degree inclined orbit at about 500 km altitude) and aim to estimate the moon's gravity field to high degree and order, the tidal Love number k_2 (including its imaginary part) and the rotational parameters (obliquity and physical librations in longitude). Such physical quantities are estimated as part of the JUICE spacecraft orbit reconstruction, relying on very accurate range and range-rate measurements provided by the 3GM Ka band Transponder (KaT), during the nearly 9 h of tracking per day that will be devoted to gravity measurements through the fixed 2.5 m High Gain Antenna (HGA). In addition, the combination of 3GM measurements along with those from the onboard GAnymede Laser Altimeter (GALA) will allow the ice viscosity and the outer shell thickness to be constrained with unprecedented accuracy, and to confirm the presence or absence of subsurface ocean (Steinbrügge et al., 2015; Moore and Schubert, 2003). The tidal quality factor, Q, will provide further information about the dissipation rate (Kamata et al., 2016), thus providing insights into the moon's energy budget and the mechanism that keeps the ocean in a liquid state (Showman et al., 1997). 3GM will also provide a precise orbit reconstruction of the spacecraft, of paramount importance in the accurate referencing of laser altimetric data (Thor et al., 2020), and will help to improve the ephemerides of the Galilean moons. The 3GM payload also includes an Ultra Stable Oscillator (USO) which will be used to carry out atmospheric occultation experiments during previous mission phases. 3GM occultation experiments are not treated in this paper.

The KaT is used to establish a two-way coherent Ka/Ka radio link (uplink at 34.5 GHz, downlink at 32.2 GHz) that will enable Doppler and range measurements as accurate as, respectively, 0.003 mm/s at 1000 s integration time and 20 cm after a few seconds of integration time (Iess and Boscagli, 2001; Asmar et al., 2005). A very similar unit is currently flying on ESA's BepiColombo mission as part of the MORE experiment (Iess et al., 2009) and likewise is manufactured by Thales Alenia Space Italy. If needed, the KaT will operate together with the Deep Space Transponder (DST) to provide a multi-frequency link. The DST adds the capability of receiving an uplink in X-band and retransmitting an X-band and a Ka-band signal back to the ground station, coherently in phase. The three simultaneous links (X/X, X/Ka, and Ka/Ka) will permit full cancellation of dispersive noise sources (Bertotti et al., 1993), mainly the interplanetary plasma and the Earth ionosphere, when the radio signal passes close to the solar corona, a situation occurring at low Sun-Earth-probe (SEP) angles. 3GM will also exploit data collected by the on-board High Accuracy Accelerometer (HAA) to calibrate the non-gravitational disturbances mainly induced by propellant sloshing in the spacecraft tanks.

3. Dynamical model

3.1. Gravity field and tidal response

The gravity potential, U, outside a body of mass M and radius R expressed in a body-fixed reference frame is given by Eq. (1) (Kaula, 1966):

$$U(r,\theta,\lambda) = -\frac{GM}{r}\left[1+\sum_{l=2}^{\infty}\sum_{m=0}^{l}\left(\frac{R}{r}\right)^{l}\overline{P}_{lm}(\sin\theta)\left[\overline{C}_{lm}\cos(m\lambda)+\overline{S}_{lm}\sin(m\lambda)\right]\right] \tag{1}$$

where (r,θ,λ) constitute the spherical coordinates (radial distance, latitude, longitude), l and m are the spherical harmonics degree and order, $\overline{P}_{lm}$ the normalized associated Legendre polynomials, and $\overline{C}_{lm}$, $\overline{S}_{lm}$ the normalized gravity coefficients. Ganymede's unnormalized quadrupole field coefficients were estimated by the Galileo spacecraft (Anderson et al., 1999) ($J_2 = (127.8 \pm 3)\cdot 10^{-6}$ and $C_{22} = (38.3 \pm 1)\cdot 10^{-6}$) using the hydrostatic constraint. Higher degree terms were not accessible, although (Palguta et al., 2006) found evidence for mass anomalies. For this reason, we adopted Kaula's rule (Kaula, 1966; Bertotti et al., 2003) to simulate higher degrees. Kaula's rule (Eq. (2)) provides the amplitude of gravity field coefficients spectra (defined by Eq. (3)). It has been proven to predict well the high order gravity field of rocky bodies but its strict applicability to icy satellites is unknown, given the absence of any data. We used a gravity field with a Kaula coefficient, A_k, of 4, derived from the model of (De Marchi et al., 2020), which simulates the moon with 7 concentric layers and considers the effect of possible density contrast of dark and bright terrains (Schenk et al., 2001). As a comparison, Titan's Kaula coefficient has been determined to be close to $A_k = 1$ (Durante et al., 2019).

$$\overline{C}_l^2 = A_k\frac{10^{-10}}{l^4} \tag{2}$$

$$\overline{C}_l^2 = \frac{1}{2l+1}\sum_m\left(\overline{C}_{lm}^2+\overline{S}_{lm}^2\right) \tag{3}$$

The synthetic $\overline{C}_{lm}$ and $\overline{S}_{lm}$ coefficients have been randomly generated up to degree and order 50 in order to fulfil Kaula's power rule. Regarding the k_2 tidal Love number, the value of 0.3 has been used, being the central value of the investigation carried out by (Kamata et al., 2016). Nevertheless, the choice of the central value does not affect the retrieved formal uncertainty.

3.2. Ganymede's exosphere

Several models describing Ganymede's neutral environment have been developed over the last decade or more. The first was provided by

(Marconi, 2007), who published a 2-D axisymmetric, kinetic model in agreement with already available observations, which showed evidence for an exosphere with two main components, O_2 and H_2O. Building on this (Turc et al., 2014), developed the first 3-D model that was in agreement with (Marconi, 2007). (Plainaki et al., 2015) combined models originally developed for Europa and Mercury and the effect of the ion precipitation using a global magnetohydrodynamic model by (Jia et al., 2009) to run a Monte Carlo simulation of a 3-D exospheric model for Ganymede. More recently (Leblanc et al., 2017), have taken into account the variability of the moon's exosphere along the moon's orbit around Jupiter.

In this work we have used the model of (Plainaki et al., 2015), in which the O_2 and H_2O exospheres are simulated through a 3-D Monte Carlo model that takes into consideration the combined effect of the main surface release processes (i.e. sputtering, sublimation and radiolysis) and the surface precipitation of the energetic ions of Jupiter's magnetosphere. For the purpose of this work, the O_2 exosphere is described by an empirical formula in (Milillo et al., 2016) which is based on EGEON, a single-particle Monte Carlo model applied to Europa (Plainaki et al., 2010, 2012, 2013), but has been adapted for Ganymede. The simulation technique for the sputtered H_2O exosphere (explained in more detail below) is based on the Monte Carlo model of (Mura et al., 2009), which was first applied to Mercury.

The production of the exosphere involves the combination of three processes (see Fig. 1). Ion sputtering: magnetospheric ions (O^+, H^+, S^+) strike the icy surface of the moon, and release H_2O; radiolysis: ionizing radiation dissociates ice into smaller particles, which are then sputtered into the exosphere, some of which react to form other exospheric species; and sublimation: on the dayside, heat from the sun causes ice to sublimate into the exosphere (Plainaki et al., 2015).

The process of simulating the exosphere of Ganymede relies on a number of assumptions about generation processes and escape rates. The release of material from the surface is expected to be determined by the flux of ion precipitation and the surface temperature. The surface temperature on Ganymede is taken to be a function of the solar zenith angle and varies between 150 K on the dayside and 80 K on the nightside, as reported by (Orton et al., 1996) from the Galileo photopolarimeter (PPR) measurements. The ion fluxes resulting from Monte Carlo simulations of the ion populations in Jupiter's magnetosphere have been scaled to match observations by Galileo (Paranicas et al., 1999). Loss rates are generally caused by reactions between plasma and neutral particles so plasma ion energies and densities are needed (Plainaki et al., 2015). used electron density values and average plasma ion energy from (Kivelson et al., 2004).

The moon's magnetic field interacts with the Jovian magnetosphere forming areas of magnetic reconnection that partially shield the underlying surface regions of the moon from ion precipitation. The ions reach Ganymede's surface through the open magnetic field lines, which are not north-south symmetric about the equator: on the trailing hemisphere side (upstream), the boundary between the open and closed magnetic field lines is at a higher latitude in comparison with the boundary on the leading hemisphere side (downstream). In addition, as Ganymede orbits Jupiter, it moves up and down within the Jupiter plasma sheet, changing the location of these boundaries (Kivelson et al., 1996). All of these factors lead to areas of preferential ion entry and precipitation onto the moon's exosphere, thereby creating an inhomogeneous sputtered exosphere. Since sublimation only occurs on the dayside, this also contributes to an overall inhomogeneous exosphere.

The exospheric model output provided by (Plainaki et al., 2015) consists only of the major constituents, O_2 and H_2O, since the minor constituents (e.g. H, OH, O) do not contribute much to the exospheric density. The H_2O exosphere contribution was provided in the form of a 3D data-array, while the O_2 exosphere is described by:

$$\log_{10}\bar{\rho}(R,\alpha) = (p_5 + p_6\cos\alpha)e^{-p_4(R-1)} - \frac{R-1}{p_1} + p_2 + p_3\cos\alpha \quad (4)$$

where $\bar{\rho}$ is the number density in m^{-3}, p_1-p_6 are free parameters, α is the subsolar angle and R is the altitude above the moon's surface, expressed in Ganymede radii. The parameters $p_1 - p_3$ mostly describe the low altitude profile, while $p_4 - p_6$ the higher altitudes. Since JUICE will stay at an altitude of roughly 500 km during this orbital phase around Ganymede, the model has been simplified by keeping R constant. Thus, Eq. (4) has been re-written as:

$$\log_{10}\bar{\rho}(R,\alpha) = A_1 + A_2\cos\alpha \quad (5)$$

where A_1 and A_2 are:

$$A_1 = p_5 e^{-p_4(R-1)} - \frac{R-1}{p_1} + p_2 = 8.35 \; A_2 = p_6 e^{-p_4(R-1)} + p_3 = 0.55 \quad (6)$$

These two parameters fully describe the exospheric O_2 density at JUICE's altitude. We have calculated that the consequences of assuming a perfectly circular orbit of 500 km, when the orbit is in fact slightly eccentric, only gives a 1–2% difference in the value of A_1 (the largest contribution to the O_2 exosphere) and is therefore insignificant. Additionally, the H_2O data array was interpolated to give the corresponding density at the specific location of the spacecraft in Ganymede's exosphere (according to altitude, latitude and longitude). Since only the model output is available instead of an analytical model, the only parameter associated with the H_2O density that can be adjusted is a scale factor.

The atmospheric drag induced by Ganymede's exosphere can be determined as part of the orbit reconstruction process:

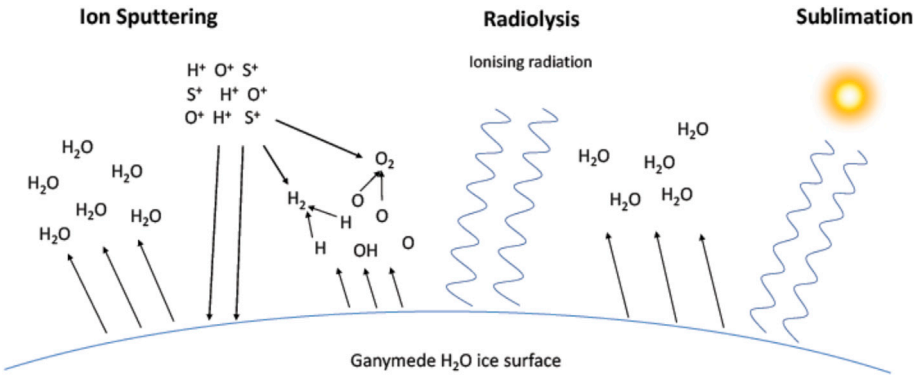

Fig. 1. Ion sputtering: magnetospheric ions bombard the surface and sputter H_2O into the exosphere (left). Radiolysis: ionizing radiation dissociates the ice into different molecules which recombine and are, in turn, sputtered into the exosphere (center). Sublimation: on the dayside, water is sublimated into the exosphere (right).

$$F_{drag} = -\frac{1}{2}\rho C_d A v_{rel}^2 \hat{v}_{rel} \quad (7)$$

where ρ is the atmospheric density measured in kg/m^3, A is the effective area of the spacecraft normal to the flow, C_d is the drag coefficient that is usually taken between 2 and 2.5 (2.1 in this case) and $\hat{v}_{rel}$ is the unit vector of the velocity relative to Ganymede's exosphere. The drag signal is modulated by the JUICE orbital period around Ganymede (about 3 h) and it has a peak amplitude of $\sim 10^{-11}$ m/s^2 (which is below the HAA measurement sensitivity). However since the effect accumulates with time, after a few orbits it induces deviations from the nominal trajectory that yield a distinctive signature in the Doppler data. Fig. 2 shows the Doppler signal due to the atmospheric drag compared to 3GM measurement accuracy at 1000 s integration time.

3.3. Propellant sloshing and HAA

Numerical simulations carried out by Airbus Defense & Space (ADS), the JUICE's prime contractor, have shown that the displacement of the propellant center of mass following attitude reorientation maneuvers can be as large as 30 cm on a timescale of $\sim$ 1000 s. The simulations have been carried out for the Europa flybys where the residual propellant mass should be about 1000 kg, compared to a dry mass of $\sim$ 2000 kg. These crude estimates show that the additive Doppler effect associated with the spacecraft buffeting is at least two orders of magnitude higher than the 3GM measurement sensitivity ($3\,\mu m/s$at 1000 s integration time, see Section 2). This effect is expected to decrease by about an order of magnitude during the Ganymede phase, depending on the residual propellant in the two tanks. Here we have assumed a residual mass of 100 kg while JUICE is in circular orbit around Ganymede, and scaled the ADS numbers by the ratio of the propellant masses. Fig. 3 shows the line-of-sight velocity induced on the spacecraft structure by propellant sloshing in the Ganymede phase. These uncalibrated accelerations would cause a degradation of the experiment performance of about a factor 10.

In order to calibrate the sloshing-induced acceleration, JUICE will house a dedicated High Accuracy Accelerometer (HAA). It is a recurrent unit, manufactured by Thales Alenia Space Italy, from the Italian Spring Accelerometer (ISA) currently flying on BepiColombo (Iafolla et al., 2010). The HAA has been slightly redesigned to cope with the harsh radiation environment of Jupiter.

The HAA measurements can be modeled as (Lucchesi and Iafolla, 2006):

$$a_{HAA} = \lambda a_{NGA} + b_0 + \varepsilon_{random} \quad (8)$$

where a_{HAA} is the total HAA reading, λ is a measurement scale factor (ideally equal to 1), a_{NGA} are the non-gravitational accelerations, b_0 is a bias error and ε_{random} is an additive random noise. According to the HAA instrument data sheet (Pecora et al., 2018), the relative measurement

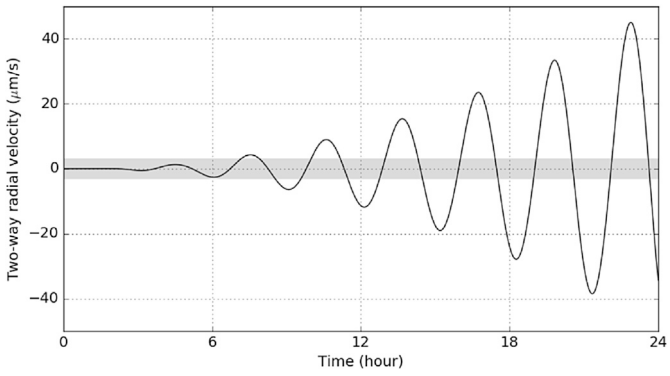

Fig. 2. The effect of Ganymede's exosphere on the two-way Doppler signal over one day. The gray region represents the Doppler measurements requirement at 1000 s integration time.

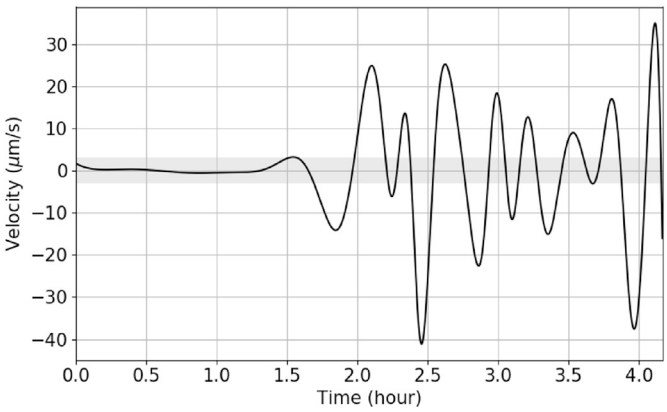

Fig. 3. Range rate noise caused by propellant sloshing on the spacecraft structure during GCO-500 projected along the line-of-sight, assuming a scaling factor on the simulation for Europa as described in the text. The gray area represents the Doppler measurement required accuracy at 1000 s integration time.

uncertainty on λ is approximately 1% and b_0 has an upper value lower than $10^{-8}\ m/s^2$ in the frequency range $[10^{-3} - 10^{-1}]Hz$. The amplitude power spectral density of the random noise ε_{random}, inferred from ISA (Iafolla et al., 2007), is assumed as in Fig. 4.

Any time the unit is switched on or off, the internal thermo-mechanical hysteresis induces unpredictable variations of λ and b_0 (within the limits stated above). Those parameters are non-deterministic, and their variability must be accounted for in the data analysis. The HAA has three different sensing elements for sampling the accelerations in three orthogonal directions. Therefore, the set of parameters to estimate is composed of: λ_X, λ_Y, λ_Z, b_{0X}, b_{0Y} and b_{0Z}.

3.4. Ephemerides model

The Galilean moons' ephemerides are based on the NOE-5-2017-GAL (Lainey et al., 2009; ESA SPICE Service, 2018), the reference for JUICE's mission analysis. The dynamical model takes into account the gravity all the planets in the Solar System and the four Galilean moons of Jupiter. Regarding the planetary ephemerides the DE430 (Folkner et al., 2014) have been considered.

4. Simulation setup

4.1. Orbit determination

The orbit determination process aims to improve the spacecraft dynamical model through the comparison of observable quantities

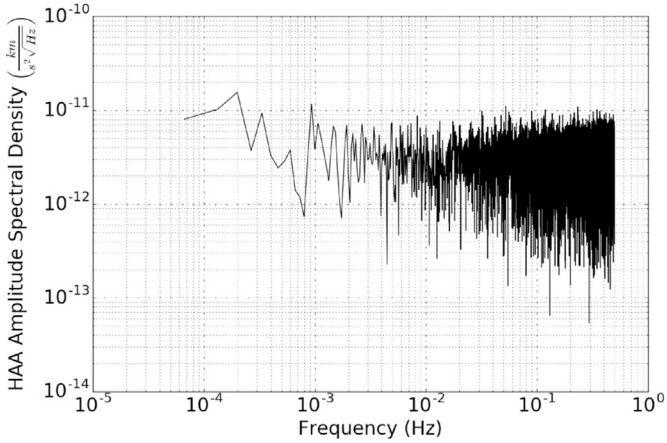

Fig. 4. HAA random noise amplitude spectral density.

Table 1
Estimated parameters with respective a priori uncertainties.

Physical quantity	Parameter	Nominal value	A priori uncertainty
JUICE state (local)	Position	taken from CReMA 4.0	Unconstrained
	Velocity	taken from CReMA 4.0	Unconstrained
Ganymede state (global)	Position	taken from NOE-5-2017-GAL	Unconstrained
	Velocity	taken from NOE-5-2017-GAL	Unconstrained
Gravity field (global)	Spherical harmonics coefficients	(Anderson et al., 1999) + Kauls's rule (see Sec. 3)	Unconstrained
Ganymede rotational parameters (global)	RA	268.2 deg (Archinal et al., 2018)	Unconstrained
	DEC	64.57 deg (Archinal et al., 2018)	Unconstrained
	Angular velocity, ω	50.32 deg/day (Archinal et al., 2018)	Unconstrained
	Libration amplitude, ϕ	0 deg	Unconstrained
Gravity tide (global)	Love number, k_2	0.3	Unconstrained
HAA parameters (global)	Scale factor, λ	1	0.01
	Bias, b_0	0	10^{-8} m/s^2
Exospheric parameters (global)	A_1	8.35	1.6
	A_2	0.545	0.545
	H_2O scale factor	1	1

(Doppler and range data computed by means of a dynamical and an observations model) and the actual measurements, forming the so called vector of residuals. A weighted least squares filter is used to minimize the square of the residuals to correct the initial state vector of the spacecraft and the other free parameters of the model, including the gravity spherical harmonic coefficients. In the classical batch filter process, the expression for the differential correction, $\delta\widehat{X}_0$, with a priori information is given by (Tapley et al., 2004):

$$\delta\widehat{\mathbf{X}}_0 = \left(H^T W H + \overline{P}_0^{-1}\right)^{-1}\left(H^T W \delta\widehat{\mathbf{y}} + \overline{P}_0^{-1}\delta\overline{\mathbf{X}}_0\right) \tag{9}$$

where H is the mapping matrix that contains the partial derivatives of the observables with respect to the solved-for parameters, W is the weighting matrix, $\mathbf{y}$ is the set of observables residuals, $\overline{P}_0$ is the a priori covariance matrix and $\delta\overline{\mathbf{X}}_0$ is deviation from the a priori estimate.

For these simulations, we have divided the GCO-500 phase into 1-day arcs and used a multi-arc approach (Milani and Gronchi, 2009). The parameters of the dynamical model that will be estimated are split into "local" parameters, which pertain to each arc, and "global" parameters, which are common to all arcs. For example, the state vector of JUICE at the beginning of each arc, taken from the notional trajectory labelled 141a of CReMA 4.0 (ESA SPICE Service, 2018), is a local parameter. Whereas, gravity coefficients are common to all arcs so are considered as global parameters. The multi-arc approach is an overparameterization suitable to cope with the dynamical model's inaccuracies, providing a faithful estimate of the free parameters.

4.2. Estimated parameters

Table 1 summarizes all the estimated parameters with the respective a priori uncertainties.

We estimated the coefficients of the gravity field's spherical harmonic expansion up to degree and order 50, including the tidal response of Ganymede to Jupiter forcing by means of the complex Love number k_2 (the imaginary part is tied to dissipation).

Since the a priori knowledge of the spacecraft state, Ganymede state, gravity field, rotational parameters and tides is poor they have been considered as unconstrained, as a conservative choice. The choice of estimating the spacecraft state every 24 h derives from the possible wheel off-loading manoeuvres that could occur between two subsequent passes, interrupting the dynamical coherence of the spacecraft trajectory.

The HAA calibration parameters have been estimated as global parameters in the orbit determination process. This assumption is true only if the unit always remains on during the entire Ganymede phase. The ideal case is if the accelerometer would always be ON during the whole mission to characterize its behavior on a longer timescale, as it baselined for BepiColombo. For JUICE, this will not be possible as power budget constraints will prevent it during the Jovian tour. On the contrary, if the HAA is continuously switched ON and OFF during subsequent passes of the Ganymede phase, two problems arise: firstly, its calibration parameters should be re-estimated at each arc (leading to an overall degradation of the estimate), and, more importantly, the instrument will have not reached thermal stability; the time needed for thermal stabilization is about 1–2 days (Lucente et al., 2018). Therefore, the HAA should always be ON during the Ganymede phase.

The O_2 exosphere parameters A_1 and A_2 (Eqs. (5) and (6)) have been initialized with a value of 8.35 and 0.545 with an a priori uncertainty of 20% and 100% of their nominal values, respectively. The H_2O density scale factor has an a priori value and an uncertainty equal to 1.0.

4.3. Synthetic observables

Range and range rate data are the primary observables for the 3GM Ganymede experiment. The range data have been simulated every 300 s with a noise jitter of 20 cm two-way. This can be considered a conservative value since recent ESA's BepiColombo MORE test in cruise has shown an unprecedented ranging jitter of less than 1 cm after 4 s integration time at an Earth-spacecraft distance of ∼ 0.3 AU (Cappuccio et al., 2019). These are preliminary results and further analysis is needed to consider them as absolute range measurements.

The 3GM requirement on the end-to-end link frequency stability, expressed in terms of the Allan deviation, is $7 \cdot 10^{-15}$ at an integration time of 1000 s. As a conservative choice, we considered an ADEV of 10^{-14}, corresponding to Doppler measurements having an accuracy of 0.003 mm/s at 1000 s. If we consider an additive white Gaussian noise, the Allan deviation at different integration times scales with the square root of the count time. Hence, at 60 s integration time the simulated noise on the observables is $\sqrt{(1000/60)}$ times larger, i.e., 12 μm/s. As per the baseline configuration of the ground system, only ESA's Deep Space Antenna 3 (DSA-3, Malargüe, Argentina) radio tracking station has been considered, corresponding to an 8–9 h tracking pass per day. So far, DSA-3 is the only ESTRACK station capable of transmitting in X and Ka-band and receiving the coherent signal sent back from the spacecraft in X and Ka. There are two coherent links in Ka-band: one coherent with the uplink X signal and the other with the radio science Ka uplink. DSS-25 (a 34 m dish located in Goldstone, California, part of NASA's Deep Space Network, DSN for short) provides another tracking option. In the simulation of the observables, a minimum spacecraft elevation angle of 15° has been adopted to account for errors that might affect low-elevation calibration data for Earth's troposphere. In addition, we considered the occultation of the radio link by Jupiter and the Galilean moons.

Table 2
Ganymede's GM and quadrupole gravity field unnormalized coefficients reconstructed uncertainties (1σ).

$GM(km^3/s^2)$	J_2	C_{21}	S_{21}	C_{22}	S_{22}
$3.8 \cdot 10^{-4}$	$8.6 \cdot 10^{-10}$	$1.7 \cdot 10^{-10}$	$7.2 \cdot 10^{-11}$	$3.0 \cdot 10^{-10}$	$5.1 \cdot 10^{-9}$

5. Results

Table 2 summarizes the predicted accuracy (1σ) on the gravitational parameter, GM, and the quadrupole field coefficients of Ganymede.

Fig. 5 shows the power spectrum of the simulated Ganymede gravity field (solid line), and the attainable formal accuracy (3σ) in the retrieval of gravity field coefficients (dashed line). Since Ganymede's true gravity field is unknown, we have also plotted two other possible gravity fields, obtained using Kaula's rule with A_k values of 0.4 and 40, corresponding to a weak field and a strong field, respectively. Even in the case of the weaker gravity signal, Ganymede's gravity field can be estimated to a degree higher than 30. On the other hand, the gravity field uncertainty is mostly independent from the gravity strength, since it mainly depends on the amount of data and on the geometry of the orbit, neither of which are subject to change. This justifies our choice of truncating the gravity field at degree and order 50.

Fig. 6 shows a Hammer-Aitoff projection map of the uncertainty on the surface gravity anomalies. The slight North-South asymmetry is a consequence of the (small) JUICE orbital eccentricity: the orbit has a pericenter in the northern region at about 475 km and an apocenter in the southern hemisphere at 525 km. The little cusps are due to the spacecraft coverage of the moon's surface.

In addition to the static gravity field, the variation of the quadrupole terms along Ganymede's orbit around Jupiter will allow the precise estimation of both the real and imaginary part of the complex k_2 Love number, as shown in Table 3. The k_2 value and phase will give us information on Ganymede's tides and thus on themoon's total internal energy dissipation (Hussmann et al., 2016). Furthermore, the pole and the rotational state of Ganymede can be estimated with a very high accuracy. The right ascension (RA) and declination (DEC) can be determined with an accuracy of 2.5 *μrad* and 1.4 *μrad*, respectively. These can be converted to an accuracy on the obliquity, *φ*, of 1 *μrad*, corresponding to 0.2 arcsec. The rotation rate, ω, of Ganymede can be obtained with an accuracy of $8.0 \cdot 10^{-14}$ rad/s, roughly 8 parts per billion of the rotational period. Here we considered only the libration, ϕ, at orbital period because it is the largest libration that can be used to infer the internal

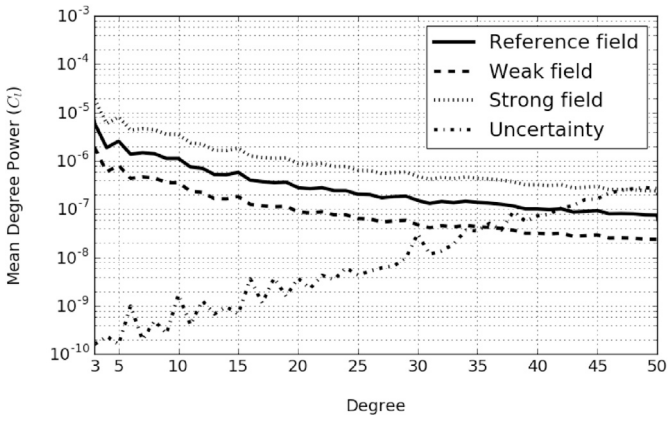

Fig. 5. Uncertainty in Ganymede's gravity power spectrum: simulated gravity field represented by a solid black line, reconstructed uncertainty (3σ) with a dashed line, strong gravity field, with Kaula's coefficient $A_k = 40$, and a weak gravity field, $A_k = 0.4$, with a dotted and broken line respectively.

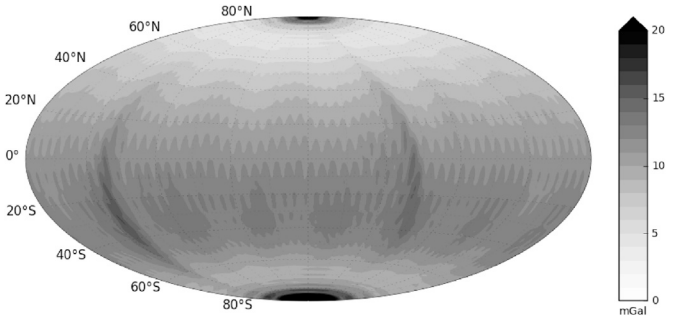

Fig. 6. Hammer-Aitoff projection map of Ganymede's gravity field uncertainty.

Table 3
Predicted accuracy in Ganymede complex k_2 Love number and rotational parameter. The RA, DEC, ω and ϕ are directly estimated, while *φ* accuracy is derived from RA and DEC.

k_2^r	k_2^i	RA (*μrad*)	DEC (*μrad*)	ω (rad/s)	ϕ (*μrad*)	*φ* (*μrad*)
$1.0 \cdot 10^{-4}$	$6.8 \cdot 10^{-5}$	2.5	1.4	$8.0 \cdot 10^{-14}$	2.1	1.0

structure of the moon (Van Hoolst et al., 2013; Rambaux et al., 2011). It is detectable at the level of 2.1 *μrad*, corresponding to 5.5 m on the equator (Steinbrügge et al., 2019). declare an expected accuracy on the outer ice shell libration, by means of GALA measurements, in the range $2.5 - 6.6$ *μrad* (6.6–17.4 m at the equator). The combination of this two values will help to decouple the total libration from the contribution of the ice-shell and to better characterize the subsurface ocean.

The process of precise orbit determination will be important to reconstruct a reference trajectory for other instrument operations. For example, the correct interpretation of laser altimetric data produced by GALA instrument requires a precise orbit reconstruction (in addition to a gravity-defined reference surface). GALA will provide the h_2 Love number (Steinbrügge et al., 2015), which, through the combination $1+ k_2 - h_2$, is a key parameter to infer the thickness of the outer icy shell (Wahr et al., 2006). h_2 is a crucial quantity to disentangle the gravity tides from the physical tides, which will likely allow an unambiguous detection of the internal core and the ocean (Kamata et al., 2016). An example of JUICE's trajectory reconstruction accuracy during an arc is shown in Fig. 7. Since the geometry of the orbits and the ground station coverage is very similar for all the 1-day arcs, the trajectory reconstruction accuracy of a single arc is representative of the whole mission time-span.

Fig. 8 shows the accuracies of Ganymede's orbit reconstruction with respect to Jupiter's barycenter in the moon's RTN (radial transverse normal) frame. The position of the moon can be reconstructed with an accuracy of tens of centimeters along the radial and transverse directions and of a few meters along the normal direction. The Ganymede semi-major axis, *a*, can be estimated with an average accuracy of $2 - 3$ cm. Given the experiment timespan, it can be converted to an accuracy on $da/dt \sim 7.\ m/century$. The information gained about the ephemerides will not only help the navigation of future missions but it is also important for studying the Jupiter system formation and evolution.

The exospheric density estimated along two JUICE orbits around Ganymede is shown in Fig. 9 together with its associated 1σ uncertainty. The exospheric density is variable along the orbit because the adopted model (Eq. (5)) is dependent on the sub-solar angle and because the sputtering contribution is inhomogeneous.

A second setup has been run by considering a diurnal variability of the exospheric density. In the process of generation of synthetic observables, a white Gaussian noise has been added on the exospheric parameters with a sigma comparable with their associated uncertainties (see Table 1). The outcome is that a constant set of exospheric parameters can absorb this variability without a significant variation of the other

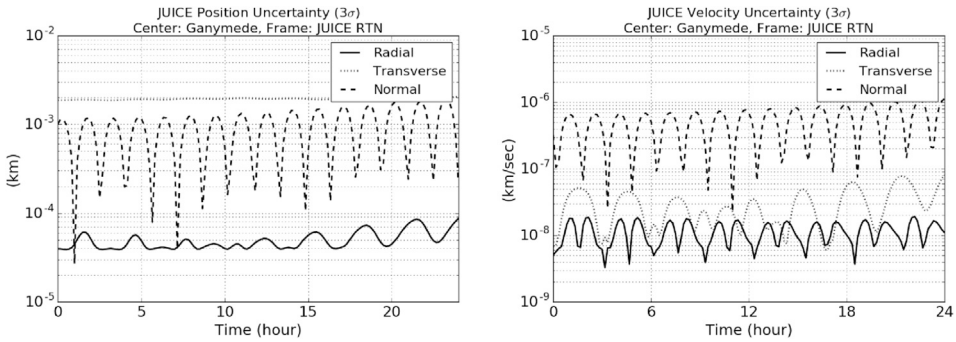

Fig. 7. JUICE reconstructed position and velocity during a 1-day arc as result of 3GM precise orbit determination. The position is expressed in km and the velocity in km/s in the JUICE RTN (radial, transverse, normal) frame pointing towards Ganymede.

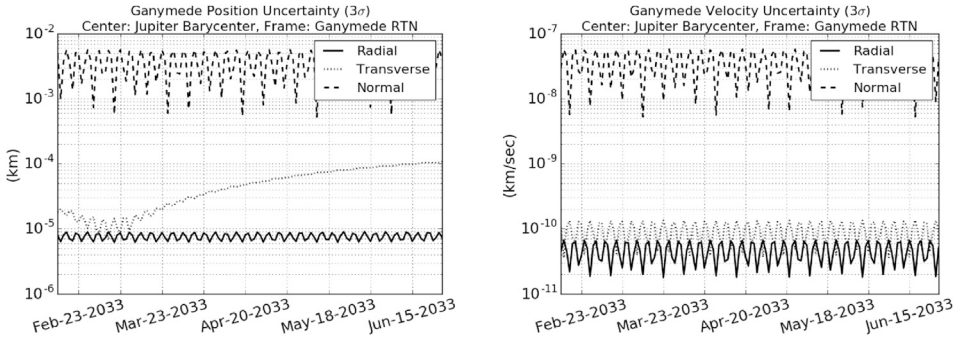

Fig. 8. Ganymede position (km) and velocity (km/s) reconstruction with respect to Jupiter barycenter expressed in the Ganymede RTN frame. Only the GCO-500 timeframe has been considered.

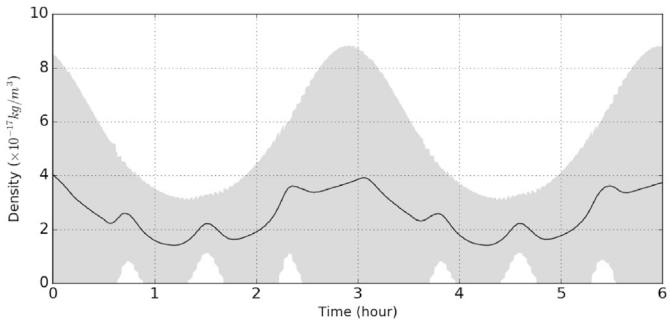

Fig. 9. The estimated exospheric density over a 6-h period on April 6, 2033. The shaded region represents the uncertainty (1σ). The corresponding drag acceleration ranges from 2 to.$6 \cdot 10^{-12} m/s^2$

estimated parameters with respect to the nominal setup. In addition, this demonstrates that the orbital fit is not sensitive to an unmodeled temporal variation of the exospheric density with a magnitude within the a priori uncertainty.

6. Conclusions

Our simulations show that the 3GM gravity experiments, in combination with other instruments, will contribute to infer Ganymede's interior structure and to provide a full characterization of the moon. The moon's gravity field can be confidently determined up to degree 35–40, together with a detailed characterization of the rotational state and the tides. The determination of the low-degree gravity coefficients along with characterization of the tidal response of the moon is crucial to determine the interior structure. Characterizing the subsurface ocean and therefore the moon's internal structure will be a joint effort by 3GM and other instruments (e.g. GALA). Higher degree gravity coefficients can be correlated with topography to determine the ice shell thickness as well as properties of the internal layers and the degree of compensation, as investigated in (De Marchi et al., 2020).

In the present analysis we do not estimate the wheel off-loading maneuvers that will occur during GCO-500 to desaturate the reaction wheels operating to contrast the gravity gradient torque. The number of these maneuvers, their frequency and uncertainty will be determined in a later stage of the project. The wheel-offloading maneuvers interrupt the dynamical coherence of the orbit preventing us from estimating the exospheric parameters and providing a continuous reconstructed trajectory. Since the frequency of those maneuvers certainly has an impact on our experiment results, they must be considered in an appropriate way. A possible strategy to cope with the problem is to use a constrained multi-arc approach: the discrepancies of spacecraft states of two subsequent arcs at the overlapping time are confined inside a specified value (Alessi et al., 2012). (Imperi et al., 2018) applied this technique to the BepiColombo case showing that it helps to mitigate the problem.

Further analysis should also consider different mission scenarios such as the possibility of a GCO-200 phase for the last part of the mission (circular orbit at an altitude of 200 km). This would certainly increase the maximum degree of the gravity field that could be trustfully reconstructed, since the gravity signal is larger at lower altitudes. The effect of the exosphere would be significantly larger, requiring a careful analysis for its assessment.

Declaration of competing interest

The authors declare that they have no known competing financial interests or personal relationships that could have appeared to influence the work reported in this paper.

CRediT authorship contribution statement

P. Cappuccio: Methodology, Software, Validation, Writing - original draft, Formal analysis. **A. Hickey:** Methodology, Software, Validation, Writing - original draft. **D. Durante:** Software, Writing - review & editing. **M. Di Benedetto:** Writing - review & editing, Supervision. **L. Iess:** Funding acquisition, Writing - review & editing, Supervision. **F. De Marchi:** Resources. **C. Plainaki:** Resources, Supervision. **A. Milillo:** Resources. **A. Mura:** Resources.

Acknowledgements

The authors would like to thank all the members of the Radio Science Laboratory of Sapienza University for the valuable discussions. This work has been partially funded by the Italian Space Agency (ASI) under the contract n. 2018-25-HH.0.

Appendix A. Supplementary data

Supplementary data to this article can be found online at https://doi.org/10.1016/j.pss.2020.104902.

References

Alessi, E.M., Cicaló, S., Milani, A., Tommei, G., 2012. Desaturation manoeuvres and precise orbit determination for the BepiColombo mission. Mon. Not. Roy. Astron. Soc. 423, 2270–2278. https://doi.org/10.1111/j.1365-2966.2012.21035.x.

Anderson, J.D., Lau, E.L., Sjogren, W.L., Schubert, G., Moore, W.B., 1999. Gravitational constraints on the internal structure of Ganymede. Nature 384, 541–543. https://doi.org/10.1038/384541a0.

Archinal, B.A., Acton, C.H., A'Hearn, M.F., Conrad, A., Consolmagno, G.J., Duxbury, T., Hestroffer, D., Hilton, J.L., Kirk, R.L., Klioner, S.A., McCarthy, D., Meech, K., Oberst, J., Ping, J., Seidelmann, P.K., Tholen, D.J., Thomas, P.C., Williams, I.P., 2018. Report of the IAU working group on cartographic coordinates and rotational elements: 2015. Celestial Mech. Dyn. Astron. 130, 22. https://doi.org/10.1007/s10569-017-9805-5.

Asmar, S.W., Armstrong, J.W., Iess, L., Tortora, P., 2005. Spacecraft Doppler tracking: noise budget and accuracy achievable in precision radio science observations. Radio Sci. 40 https://doi.org/10.1029/2004RS003101.

Barth, C.A., Hord, C.W., Stewart, A.I.F., Pryor, W.R., Simmons, K.E., McClintock, W.E., Ajello, J.M., Naviaux, K.L., Aiello, J.J., 1997. Galileo ultraviolet spectrometer observations of atomic hydrogen in the atmosphere of Ganymede. Geophys. Res. Lett. 24, 2147–2150. https://doi.org/10.1029/97GL01927.

Bertotti, B., Comoretto, G., Iess, L., 1993. Doppler tracking of spacecraft with multi-frequency links. Astron. Astrophys. 269, 608–616.

Bertotti, B., Farinella, P., Vokrouhlicky, D., 2003. Physics of the Solar System. Springer Netherlands, Dordrecht.

Cappuccio, P., Di Benedetto, M., Cascioli, G., Iess, L., 2018. Analysis of the 3GM gravity experiment of ESA's JUICE mission. Adv. Astronaut. Sci. 167, 3551–3561.

Cappuccio, P., Notaro, V., Iess, L., Asmar, S., Border, J., Ciarcia, S., Di Ruscio, A., Montagnon, E., De Vicente, J., Mercolino, M., et al., 2019. First results from cruise tests of the Mercury Orbiter Radio science Experiment (MORE) of ESA's BepiColombo mission. In: AGU Fall Meeting 2019. AGU.

De Marchi, F., Di Achille, G., Mitri, G., Cappuccio, P., di Stefano, I., Di Benedetto, M., Iess, L., 2020. Observability of Ganymede's gravity anomalies related to surface features by the 3GM experiment onboard ESA's JUpiter ICy moons Explorer (JUICE) mission. Submitted to Icarus.

Di Ruscio, A., Cappuccio, P., Notaro, V., Di Benedetto, M., 2019. Improvements in BepiColombo and JUICE radio science experiments with a multi-station tracking configuration for the reduction of Doppler noise. In: Proceedings of the International Astronautical Congress. IAC.

Durante, D., Hemingway, D., Racioppa, P., Iess, L., Stevenson, D., 2019. Titan's gravity field and interior structure after Cassini. Icarus 326, 123–132. https://doi.org/10.1016/j.icarus.2019.03.003.

ESA SPICE Service, 2018. JUICE operational SPICE kernel dataset. In: Operational SPICE Kernel Dataset. https://doi.org/10.5270/esa-ybmj68p.

Folkner, W.M., Williams, J.G., Boggs, D.H., Park, R.S., Kuchynka, P., 2014. The Planetary and Lunar Ephemerides DE430 and DE431. IPN Progress Report 42-198.

Grasset, O., Dougherty, M., Coustenis, A., Bunce, E., Erd, C., Titov, D., Blanc, M., Coates, A., Drossart, P., Fletcher, L., Hussmann, H., Jaumann, R., Krupp, N., Lebreton, J.P., Prieto-Ballesteros, O., Tortora, P., Tosi, F., Van Hoolst, T., 2013. JUpiter ICy moons Explorer (JUICE): an ESA mission to orbit Ganymede and to characterise the Jupiter system. Planet. Space Sci. 78, 1–21. https://doi.org/10.1016/j.pss.2012.12.002.

Hall, D.T., Feldman, P.D., McGrath, M.A., Strobel, D.F., 1998. The far-ultraviolet oxygen airglow of Europa and Ganymede. Astrophys. J. 499, 475–481. https://doi.org/10.1086/305604.

Hussmann, H., Shoji, D., Steinbrügge, G., Stark, A., Sohl, F., 2016. Constraints on dissipation in the deep interiors of Ganymede and Europa from tidal phase-lags. Celestial Mech. Dyn. Astron. 126, 131–144. https://doi.org/10.1007/s10569-016-9721-0.

Iafolla, V., Fiorenza, E., Lefevre, C., Morbidini, A., Nozzoli, S., Peron, R., Persichini, M., Reale, A., Santoli, F., 2010. Italian spring accelerometer (ISA): a fundamental support to BepiColombo radio science experiments. Planet. Space Sci. 58, 300–308. https://doi.org/10.1016/j.pss.2009.04.005.

Iafolla, V., Lucchesi, D.M., Nozzoli, S., Santoli, F., 2007. ISA accelerometer onboard the Mercury Planetary Orbiter: error budget. Celestial Mech. Dyn. Astron. 97, 165–187. https://doi.org/10.1007/s10569-006-9059-0.

Iess, L., Asmar, S., Tortora, P., 2009. MORE: an advanced tracking experiment for the exploration of Mercury with the mission BepiColombo. Acta Astronaut. 65, 666–675. https://doi.org/10.1016/j.actaastro.2009.01.049.

Iess, L., Boscagli, G., 2001. Advanced radio science instrumentation for the mission BepiColombo to Mercury. Planet. Space Sci. 49, 1597–1608. https://doi.org/10.1016/S0032-0633(01)00096-4.

Imperi, L., Iess, L., Mariani, M.J., 2018. An analysis of the geodesy and relativity experiments of BepiColombo. Icarus 301, 9–25. https://doi.org/10.1016/j.icarus.2017.09.008.

Ip, W.H., Williams, D.J., McEntire, R.W., Mauk, B., 1997. Energetic ion sputtering effects at Ganymede. Geophys. Res. Lett. 24, 2631–2634. https://doi.org/10.1029/97GL02814.

Jia, X., Walker, R.J., Kivelson, M.G., Khurana, K.K., Linker, J.A., 2009. Properties of Ganymede's magnetosphere inferred from improved three-dimensional MHD simulations. J. Geophys. Res.: Space Phys. 114 https://doi.org/10.1029/2009JA014375.

Kamata, S., Kimura, J., Matsumoto, K., Nimmo, F., Kuramoto, K., Namiki, N., 2016. Tidal deformation of Ganymede: sensitivity of Love numbers on the interior structure. J. Geophys. Res.: Planets 121, 1362–1375. https://doi.org/10.1002/2016JE005071.

Kaula, W.M., 1966. Theory of Satellite Geodesy. Blaisdell.

Kimura, J., Nakagawa, T., Kurita, K., 2009. Size and compositional constraints of Ganymede's metallic core for driving an active dynamo. Icarus 202, 216–224. https://doi.org/10.1016/j.icarus.2009.02.026.

Kivelson, M., Khurana, K., Russell, C., Walker, R., Warnecke, J., Coroniti, F., Polanskey, C., Southwood, D., Schubert, G., 1996. Discovery of Ganymede's magnetic field by the Galileo spacecraft. Nature 384, 537–541. https://doi.org/10.1038/384537a0.

Kivelson, M.G., Bagenal, F., Kurth, W.S., Neubauer, F.M., Paranicas, C., Saur, J., 2004. Magnetospheric interactions with satellites. Jupiter: Planet Satellites Magnetosphere 513–536.

Lainey, V., Arlot, J.E., Karatekin, O., Van Hoolst, T., 2009. Strong tidal dissipation in Io and Jupiter from astrometric observations. Nature 459, 957–959. https://doi.org/10.1038/nature08108.

Leblanc, F., Oza, A., Leclercq, L., Schmidt, C., Cassidy, T., Modolo, R., Chaufray, J., Johnson, R., 2017. On the orbital variability of Ganymede's atmosphere. Icarus 293, 185–198. https://doi.org/10.1016/j.icarus.2017.04.025.

Lucchesi, D.M., Iafolla, V., 2006. The Non-Gravitational Perturbations impact on the BepiColombo Radio Science Experiment and the key role of the ISA accelerometer: direct solar radiation and albedo effects. Celestial Mech. Dyn. Astron. 96, 99–127. https://doi.org/10.1007/s10569-006-9034-9.

Lucente, M., Santoli, F., Pecora, M., 2018. JUICE HAA High Accuracy Accelerometer (HAA) Calibration Plan. JUI-IAPS-HAA-PL-000005 2.

Marconi, M., 2007. A kinetic model of Ganymede's atmosphere. Icarus 190, 155–174. https://doi.org/10.1016/j.icarus.2007.02.016.

Matsuyama, I., Nimmo, F., 2009. Gravity and tectonic patterns of Mercury: effect of tidal deformation, spin-orbit resonance, nonzero eccentricity, despinning, and reorientation. J. Geophys. Res.: Planets 114. https://doi.org/10.1029/2008JE003252.

McCord, T.B., Hansen, G.B., Hibbitts, C.A., 2001. Hydrated salt minerals on Ganymede's surface: evidence of an ocean below. Science 292, 1523–1525. https://doi.org/10.1126/science.1059916.

Milani, A., Gronchi, G., 2009. Theory of Orbit Determination. Cambridge University Press. https://doi.org/10.1017/CBO9781139175371.

Milillo, A., Plainaki, C., Angelis, E.D., Mangano, V., Massetti, S., Mura, A., Orsini, S., Rispoli, R., 2016. Analytical model of Europa's O2 exosphere. Planet. Space Sci. 130, 3–13. https://doi.org/10.1016/j.pss.2015.10.011.

Moore, W.B., Schubert, G., 2003. The tidal response of Ganymede and Callisto with and without liquid water oceans. Icarus 166, 223–226. https://doi.org/10.1016/j.icarus.2003.07.001.

Mura, A., Wurz, P., Lichtenegger, H.I., Schleicher, H., Lammer, H., Delcourt, D., Milillo, A., Orsini, S., Massetti, S., Khodachenko, M.L., 2009. The sodium exosphere of Mercury: comparison between observations during Mercury's transit and model results. Icarus 200, 1–11.

Orton, G., Spencer, J., Travis, L., Martin, T., Tamppari, L., 1996. Galileo photopolarimeter-radiometer observations of Jupiter and the Galilean satellites. Science 274, 389–391.

Palguta, J., Anderson, J.D., Schubert, G., Moore, W.B., 2006. Mass anomalies on Ganymede. Icarus 180, 428–441. https://doi.org/10.1016/j.icarus.2005.08.020.

Paranicas, C., Paterson, W., Cheng, A., Mauk, B., McEntire, R., Frank, L., Williams, D., 1999. Energetic particle observations near Ganymede. J. Geophys. Res.: Space Phys. 104, 17459–17469.

Pecora, M., Scaramella, D., Falcetti, G., M, P.J., Fumagalli, M., M, B., 2018. High Accuracy Accelerometer (HAA) Performance Requirement Assessment. JUI-TASM-HAA-AN-000001 2.

Plainaki, C., Milillo, A., Massetti, S., Mura, A., Jia, X., Orsini, S., Mangano, V., Angelis, E.D., Rispoli, R., 2015. The H2O and O2 exospheres of Ganymede: the result

of a complex interaction between the jovian magnetospheric ions and the icy moon. Icarus 245, 306–319. https://doi.org/10.1016/j.icarus.2014.09.018.
Plainaki, C., Milillo, A., Mura, A., Orsini, S., Cassidy, T., 2010. Neutral particle release from Europa's surface. Icarus 210, 385–395.
Plainaki, C., Milillo, A., Mura, A., Orsini, S., Massetti, S., Cassidy, T., 2012. The role of sputtering and radiolysis in the generation of Europa exosphere. Icarus 218, 956–966.
Plainaki, C., Milillo, A., Mura, A., Saur, J., Orsini, S., Massetti, S., 2013. Exospheric O2 densities at Europa during different orbital phases. Planet. Space Sci. 88, 42–52.
Rambaux, N., Van Hoolst, T., Karatekin, Ö., 2011. Librational response of Europa, Ganymede, and Callisto with an ocean for a non-Keplerian orbit. Astron. Astrophys. 527, A118. https://doi.org/10.1051/0004-6361/201015304.
Saur, J., Duling, S., Roth, L., Jia, X., Strobel, D.F., Feldman, P.D., Christensen, U.R., Retherford, K.D., McGrath, M.A., Musacchio, F., Wennmacher, A., Neubauer, F.M., Simon, S., Hartkorn, O., 2015. The search for a subsurface ocean in Ganymede with Hubble Space Telescope observations of its auroral ovals. J. Geophys. Res.: Space Phys. 120, 1715–1737. https://doi.org/10.1002/2014JA020778.
Schenk, P.M., McKinnon, W.B., Gwynn, D., Moore, J.M., 2001. Flooding of Ganymede's bright terrains by low-viscosity water-ice lavas. Nature 410, 57–60.
Showman, A.P., Malhotra, R., 1997. Tidal evolution into the Laplace resonance and the resurfacing of Ganymede. Icarus 127, 93–111. https://doi.org/10.1006/icar.1996.5669.
Showman, A.P., Malhotra, R., 1999. The Galilean satellites. Science 286, 77–84. https://doi.org/10.1126/science.286.5437.77.
Showman, A.P., Stevenson, D.J., Malhotra, R., 1997. Coupled orbital and thermal evolution of Ganymede. Icarus 129, 367–383. https://doi.org/10.1006/icar.1997.5778.
Steinbrügge, G., Stark, A., Hussmann, H., Sohl, F., Oberst, J., 2015. Measuring tidal deformations by laser altimetry. A performance model for the Ganymede Laser Altimeter. Planet. Space Sci. 117, 184–191. https://doi.org/10.1016/j.pss.2015.06.013.
Steinbrügge, G., Steinke, T., Thor, R., Stark, A., Hussmann, H., 2019. Measuring Ganymede's librations with laser altimetry. Geosciences 9. https://doi.org/10.3390/geosciences9070320.
Tapley, B.D., Schutz, B.E., Born, G.H., 2004. Statistical Orbit Determination. Academic Press.
Thor, R.N., Kallenbach, R., Christensen, U.R., Stark, A., Steinbrügge, G., Di Ruscio, A., Cappuccio, P., Iess, L., Hussmann, H., Oberst, J., 2020. Prospects for measuring mercury's tidal love number h2 with the bepicolombo laser altimeter. A&A 633, A85. https://doi.org/10.1051/0004-6361/201936517.
Titov, D., Grasset, O., Fletcher, L., 2014. JUICE Science Requirements Document, vol. 2. JUI-EST-SGS-RS-001, p. 5.
Turc, L., Leclercq, L., Leblanc, F., Modolo, R., Chaufray, J.Y., 2014. Modelling Ganymede's neutral environment: a 3D test-particle simulation. Icarus 229, 157–169. https://doi.org/10.1016/j.icarus.2013.11.005.
Van Hoolst, T., Baland, R.M., Trinh, A., 2013. On the librations and tides of large icy satellites. Icarus 226, 299–315. https://doi.org/10.1016/j.icarus.2013.05.036.
Wahr, J.M., Zuber, M.T., Smith, D.E., Lunine, J.I., 2006. Tides on Europa, and the thickness of Europa's icy shell. J. Geophys. Res.: Planets 111. https://doi.org/10.1029/2006JE002729.